

UNIQUE EXTRAGALACTIC SIGHTLINES: DISSECTING THE EXTREME CIRCUMSTELLAR ENVIRONMENT OF TWO γ -RAY BURST PROGENITORS WITH ECHELLE SPECTROSCOPY

JASON X. PROCHASKA¹, HSIAO-WEN CHEN², AND JOSHUA S. BLOOM³
Submitted to ApJ: December 20, 2005

ABSTRACT

High-resolution absorption line spectroscopy of the afterglows for γ -ray bursts GRB 051111 ($z_{\text{GRB}} = 1.54948$) and GRB 050730 ($z_{\text{GRB}} = 3.96855$) have unveiled extreme physical conditions in the circumburst environment that are rarely seen even in the ISM of the Milky Way. A detailed study of fine-structure transitions of Fe^+ and Si^+ and atomic transitions of Mg^0 and Fe^0 yields strong constraints on the density and temperature of the gas, as well as on the ambient radiation field. We derive, based on the large abundances of Si^+ and Fe^+ in the excited states, that the electron density n_e exceeds 10^3 cm^{-3} and argue that $n_H > 10^5 \text{ cm}^{-3}$. In addition, the excited states are populated according to a Boltzmann distribution with excitation temperature $T_{\text{Ex}} \sim 2000 - 6000 \text{ K}$. For GRB 051111, our analysis of the neutral species and excited ions identifies two spatially distinct gaseous clouds that are responsible for producing the absorption spectrum: one that gives rise to the observed fine structure transitions and the other that gives rise to the majority of the observed resonance transitions. The detection of strong Mg^0 absorption indicates the the majority of the gas associated with the ground-state is located far from the GRB ($r > 100 \text{ pc}$; likely outside the star-forming region hosting the GRB) otherwise it would have been ionized by the afterglow. In contrast, we argue the excited ions arise in a circumstellar medium local to the progenitor, $r < 10 \text{ pc}$. Our study therefore represents the first analysis of the kinematics, chemical abundances, and gas densities in a circumburst environment. The low velocity spread of the fine-structure transitions suggest the high density environment is, as we surmise, due to the interaction of a Wolf-Rayet wind with the ISM of the star-forming region. In this context, we draw comparisons between the properties of the circumburst environment with observations of gas in the vicinity of η Carinae.

Subject headings: gamma-ray bursts

1. INTRODUCTION

Optical afterglows of long-duration γ -ray bursts (GRBs) are almost certainly signposts of extreme star-forming regions at high redshift, because these bursts originate in the catastrophic death of massive stars (e.g. Woosley 1993; Paczyński 1998; Bloom *et al.* 2002; Stanek *et al.* 2003). A detailed study of metal absorption features identified in the circumburst environment can, in principle, yield strong constraints on the progenitor (e.g. Perna & Loeb 1998; Ramirez-Ruiz *et al.* 2005; van Marle, Langer & Garcia-Segura 2005) and offer important insights for understanding mass-loss and chemical feedback during the final evolution stages of massive stars (Wijers 2001; Vink 2005). The benefit of GRBs embedded in environments of Wolf-Rayet stars is that they provide extremely bright lighthouses at moderate to high redshift, allowing redshifted UV lines to be (albeit transiently) observable with high resolution spectroscopy.

Past studies based on low-resolution afterglow spectra have been limited to a few diagnostic measurements such as the H I column density, the gas metallicity, and the dust-to-gas ratio (e.g. Savaglio, Fall & Fiore 2003; Vreeswijk *et al.* 2004). In contrast, high-resolution spectroscopy of GRB afterglows has uncovered detailed kinematic signatures, population ratios of excited ions, and chemical com-

positions of the interstellar medium (ISM) and the circumstellar medium (CSM) of the progenitor star of the GRB (?Chen *et al.* 2005). These quantities, in principle, permit direct comparisons with simulations describing the evolution history of GRB progenitors (e.g. van Marle, Langer & Garcia-Segura 2005).

An emerging feature of GRB progenitor environments is the presence of strong fine-structure transitions from excited states of C^+ , Si^+ , O^0 , and Fe^+ (Chen *et al.* 2005). In contrast to resonance transitions of the dominant ions in neutral gas, these absorption lines can reveal the temperature and density of the gas, as well as the ambient radiation field (Bahcall & Wolf 1968). Perhaps more notable, detections of Fe II fine structure transitions have only been reported in rare places such as broad absorption-line (BAL) quasars (Hall *et al.* 2002), η Carinae (Gull *et al.* 2005; Nielsen, Gull & Vieira Kober 2005) and the circumstellar disk of β Pictoris (Lagrange-Henri, Vidal-Madjar & Ferlet 1988). Identifications of strong Fe II fine-structure transitions therefore suggest extreme gas density and temperature in the GRB progenitor environment.

In this paper we present a comprehensive study of the physical properties of the ISM in GRB host galaxies, using absorption lines identified in the echelle spectra of two GRB afterglows, GRB 051111 and GRB 050730. We investigate the excitation mechanism of the absorbing gas and compare the predicted population ratios with observations of different ions under either collisional excitation or photon pumping scenarios. Comparisons between different excited states allow us to rule out direct IR and indirect UV photon pumping as important mechanisms for excitation. Instead, we demonstrate that all the observed

¹UCO/Lick Observatory; University of California, Santa Cruz; Santa Cruz, CA 95064; xavier@ucolick.org

²Department of Astronomy & Astrophysics; University of Chicago; 5640 S. Ellis Ave., Chicago, IL 60637; hchen@oddjob.uchicago.edu

³Department of Astronomy, 601 Campbell Hall, University of California, Berkeley, CA 94720-3411

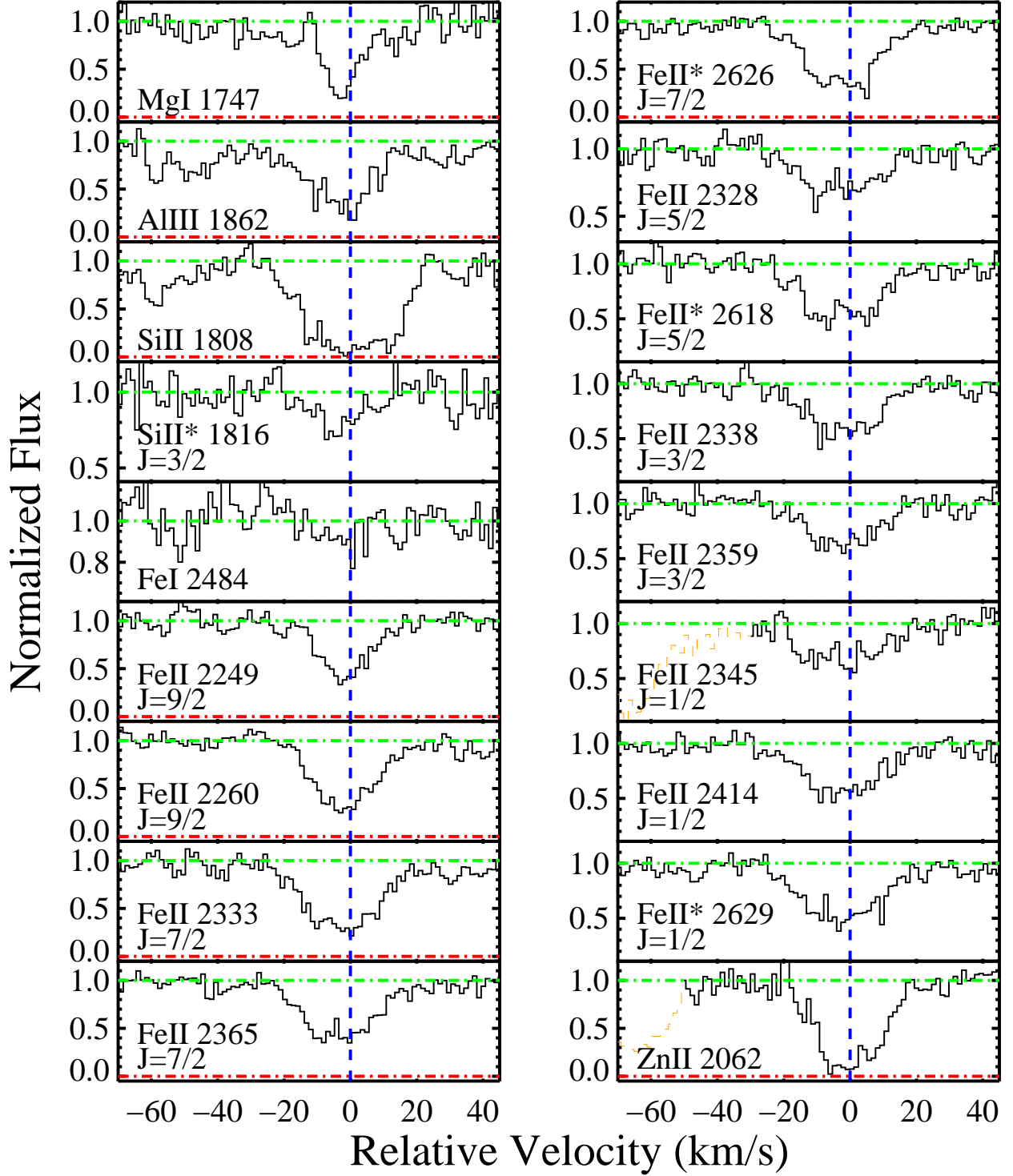


FIG. 1.— Velocity profiles for transitions arising from gas in the host galaxy of GRB 051111. The vertical dashed line at $v = 0$ corresponds to $z = 1.5495$ and the dotted lines indicate blends with coincident transitions.

fine structure transitions can be explained by a single excitation mechanism: collisions due to electrons with density $n_e \gtrsim 10^3 \text{ cm}^{-3}$ and temperature $T \sim 3000 \text{ K}$. Based on the derived physical properties, we argue that the gas is located in the immediate progenitor environment. Finally, we discuss implications for the GRB progenitors based on the derived gas density, temperature, and chemical compositions.

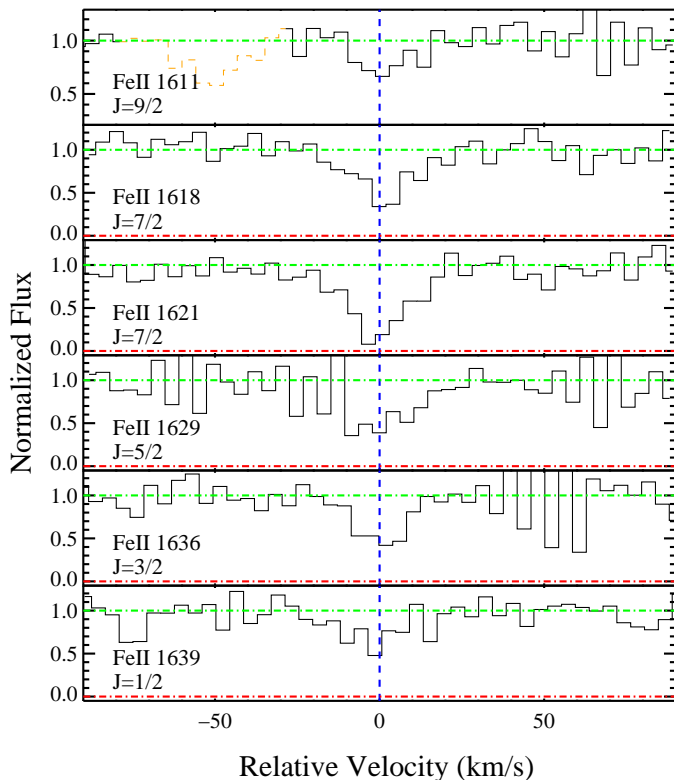


FIG. 2.— Velocity profiles for Fe II transitions arising from gas in the host galaxy of GRB 050730. The vertical dashed line at $v = 0$ corresponds to $z = 3.96855$ and the dotted lines indicate blends with coincident transitions.

2. OBSERVATIONS AND COLUMN DENSITIES

Echelle spectroscopic observations of GRB 051111 were obtained using the High Resolution Echelle Spectrometer (HIRES; Vogt *et al.* 1994) on the Keck I telescope. The observations consisted of three exposures of 1800 s duration each and were initiated by the Keck Observatory staff at UT 07:02:57.92 on 11 November 2005. The spectra⁴ covered a wavelength range from $\lambda = 4165 - 8720 \text{ \AA}$ with a spectral FWHM resolution of $\approx 5 \text{ km s}^{-1}$. A detailed description of the data reduction is presented in a separate paper (Prochaska *et al.* 2006, in preparation). The final coadded spectrum was normalized to a unit continuum and has $\text{SNR} \approx 15$ per 1.3 km s^{-1} pixel. Figure 1 presents the subset of transitions related to the GRB for the analysis performed in this paper. We (Hill *et al.* 2005) reported the discovery of the redshift $z = 1.549$ for GRB 051111 and preliminary analysis of the results Prochaska (2005).

⁴The data are publically available at <http://www.graasp.org>

Berger *et al.* (2005) and Penprase *et al.* (2005) present an independent analysis of the same data.

Echelle spectroscopic observations of GRB 050730 were obtained using the MIKE echelle spectrograph (Bernstein *et al.* 2003) on the Magellan Clay telescope. A detailed description of the observation and data reduction is presented in Chen *et al.* (2005). In addition to the absorption features presented in Chen *et al.*, here we also present identifications of Fe II transitions from excited fine structure states, $3d^6 4s^6 D_{J=5/2,3/2,1/2}$ (Figure 2).

Column densities of the unblended transitions were measured using the apparent optical depth method (AODM; Savage & Sembach 1991; Jenkins 1996) over a velocity interval $\pm 40 \text{ km s}^{-1}$ centered at $z = 3.96855$ for GRB 050730 and at $z = 1.54948$ for GRB 051111. In Tables 1 & 2, we list the column densities of individual transitions, the 1σ statistical uncertainty, and the weighted mean. In addition, we report conservative lower limits for saturated transitions and 3σ upper limits for non-detections. No systematic trend between column density and oscillator strength is identified in the measurements, indicating that the absorption lines are well resolved and that the column density measurements are robust. We note, however, that uncertainties in the continuum level are large for features with rest-frame absorption equivalent width $< 10 \text{ m\AA}$. In spite of a formal statistical error < 0.01 dex in several cases, we adopt a minimum 1σ error of 5% in subsequent analyses.

3. GASEOUS PROPERTIES AS CONSTRAINED BY FINE-STRUCTURE TRANSITIONS

Figures 1 and 2 present the velocity profiles of a subset of the resonance and fine-structure transitions originated in the progenitor environment of GRB 051111 and GRB 050730, respectively. A striking feature in both GRB hosts is the presence of Fe II and Si II fine-structure transitions which have never been observed in intervening quasar absorption line systems (e.g. Howk, Wolfe & Prochaska 2005). In Figure 3 we show the apparent optical depth profiles for all five a^6D levels of Fe^+ for GRB 051111. The velocity profiles of the excited states track each other very closely, i.e. the relative abundance is constant over this velocity range. The consistent absorption profiles of transitions from the excited 6D_J states of Fe^+ demonstrate that these ions reside in the same medium surrounding the burst progenitors and their population ratios may reflect the excitation temperature of the absorbing gas. However, the ground state does not directly track the excited states; we will return to this point in § 3.3.

In the following sections, we examine different excitation mechanisms for producing the excited states of Fe^+ and Si^+ . In addition, we determine the physical properties of the absorbing gas, such as the temperature and particle density. In several instances, we draw comparisons with model predictions calculated from the PopRatio software package (Silva & Viegas 2002) which uses the most recent atomic data for Fe^+ and Si^+ .

3.1. Collisional excitation or Photon Pumping?

Four physical processes may be responsible for producing the excited states of Fe^+ and Si^+ : (1) collisions with charged particles, primarily electrons; (2) collisions with neutral hydrogen; (3) direct pumping by IR radiation from

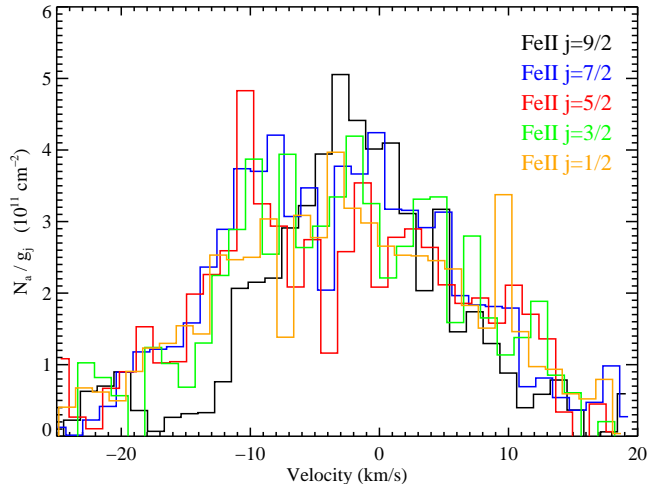


FIG. 3.— Apparent optical depth profiles of one transition from each of the five ${}^6D_{9/2}$ levels of Fe II for GRB 051111. One notes that the excited states track one another closely but that the ground state exhibits greater optical depth at $v > 0$ km s $^{-1}$ relative to the excited states. Note the $J = 9/2$ values are scaled down by a factor of 20 for comparison with the excited states.

sources local to the gas⁵ ($\lambda \approx 1 \mu\text{m}$ for Fe $^+$); and (4) fluorescence following excitations by ultraviolet pumping.

We note first that fluorescence to the Fe II ${}^6D_{1/2}$ and ${}^6D_{3/2}$ levels following excitations by UV pumping are negligible because these are forbidden by electric dipole transitions. This is a critical point for an absorbing medium local to the GRB event, because UV pumping from a star-forming region and/or the prompt emission of the burst could be significant. Furthermore, UV pumping for Si $^+$ has a minor effect because even the Si II 1808 transition is optically thick (Sarazin, Rybicki & Flannery 1979).

Direct IR pumping is a more likely process as the dominant excitation mechanism for the fine-structure states. If IR pumping dominates, then the excitation of level j relative to the ground-state i is given by

$$\frac{n_j}{n_i} = \frac{g_j}{g_i} \frac{N_\gamma}{1 + N_\gamma} \quad (1)$$

where N_γ is the number of photons at the appropriate frequency

$$N_\gamma = \frac{I_\nu \lambda^3}{8\pi h c} \quad (2)$$

But direct IR pumping from the ground states of Si $^+$ and Fe $^+$ is only permitted⁶ to Si II ${}^2P_{3/2}$ and Fe II ${}^6D_{7/2}$, respectively. To populate the other Fe II excited states requires a cascade from $J = 9/2$ to $7/2$ to $5/2$ and eventually $J = 1/2$. Adopting the photon densities necessary to populate Si II ${}^2P_{3/2}$ and Fe II ${}^6D_{7/2}$ leads to a lower limit to the spectral index α of the ambient radiation field with $I_\nu \propto \nu^\alpha$. From the observations of GRB 051111, we derive $\alpha > 3$, which is inconsistent with any thermal source, e.g. dust reradiation in a star forming region. This spectral index is also inconsistent with that observed for

⁵Note that the CMB temperature and photon density at $z = 1.5495$ cannot account for significant external IR pumping.

⁶Via forbidden magnetic dipole transitions.

the GRB afterglow at optical wavelengths (Butler et al. 2006, in prep.). Furthermore, it would be an astonishing coincidence for the radiation field to populate the Fe $^+$ ions according to a nearly Boltzmann population. We therefore rule out IR pumping for the excitation of Fe $^+$ and Si $^+$.

3.2. Excitation Temperature

If the excitations of Fe $^+$ are dominated by collisions, the relative populations yield the excitation temperature and therefore the kinetic temperature under the assumption of thermal equilibrium. Here we consider collisional excitations by electrons to be the dominant process for populating the excited fine structure, because neutral hydrogen atoms have significantly smaller cross section than charged particles. We caution, however, that the neutral collision rates for Fe $^+$ have not yet been precisely calculated or measured in the laboratory.

The population ratios between different states are determined based on the balance between excitation and de-excitation decay rates. When the density is sufficiently large that the collisional de-excitation rates exceed the spontaneous decay rate, the excited states are populated according to a Boltzmann distribution,

$$\frac{n_i}{n_j} = \frac{g_i}{g_j} \exp[-(E_{ij}/k)/T_{Ex}] \quad , \quad (3)$$

where g_i is the degeneracy of state i , $E_{ij} \equiv E_i - E_j$ is the difference in energy between the two states, and T_{Ex} is the excitation temperature. Comparing predictions following Equation (1) with the observed column densities of ions at different excited states allows us to examine whether collisional equilibrium is a representative model for the excitation mechanism. A consistent fit in turn leads to a strong constraint for the gas temperature.

Figure 4 shows for GRB051111 the observed column densities scaled by the corresponding degeneracy N_i/g_i for the Fe II excited states as a function of the energy E_{ij} above the ground state $J = 9/2$. The error bars reflect 1- σ uncertainty in N_i . The modest decrease of N_i/g_i with E_{ij} suggests the levels are Boltzmann populated with an excitation energy greater than the largest E_{ij} value. The solid (blue) curve indicates the best-fit Boltzmann function with a best-fit excitation temperature $T_{Ex} = 2600$ K. The inset shows the minimum χ^2 values as a function of T_{Ex} ; the 99% c.l. limits are $T_{Ex}(99\%) = 1800 - 6000$ K. The reduced χ^2 is nearly unity, $\chi^2_\nu = 1.02$, supporting our assumption that the Boltzmann function is a representative model. We argue in the next section this is a unique solution and, therefore, that the excitation temperature from this analysis is characteristic of the fine-structure gas.

We have repeated this analysis for GRB 050730 and the results are presented in Figure 5. The column density measurements have larger uncertainty and therefore place weaker constraints for the model. Nevertheless, the Fe $^+$ excited state population is well fit by a Boltzmann function with $T_{Ex} \approx 6000$ K with a firm lower limit of 1000 K.

3.3. Electron Density

Adopting the best-fit temperature for the absorbing medium, we can further constrain the electron density based on the observed column density ratios. We calculate the expected population ratio between excited fine structure states i and

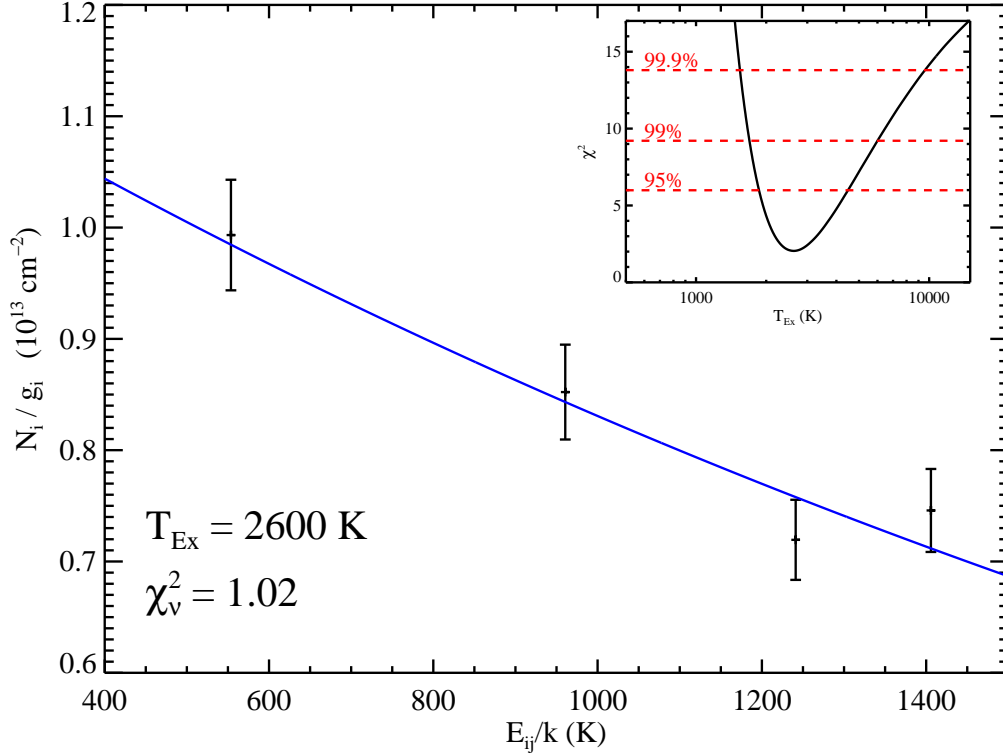


FIG. 4.— Plot of N_i/g_i for the Fe^+ excited states toward GRB 051111 as a function of their energy E_i above the ground state. Overplotted on the figure is the function $A \exp[-(E_{ij}/k)/T_{Ex}]$ for a minimum χ^2 value of $T_{Ex} = 2600 \text{ K}$. The inset shows the reduced χ^2 values for the best fit for a range of T_{Ex} values.

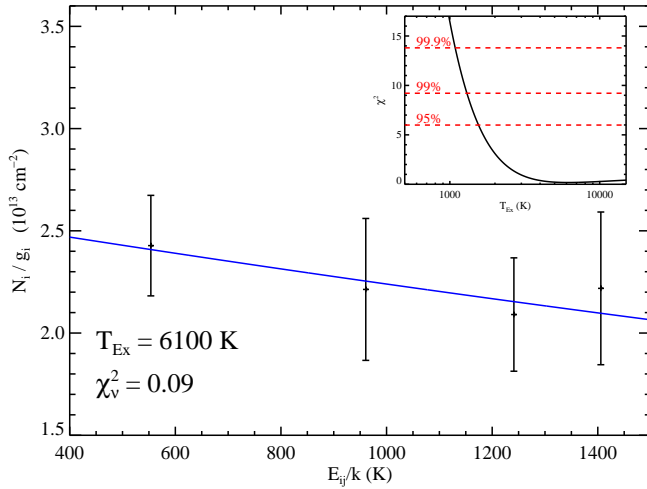


FIG. 5.— Same as Figure 4 except for GRB 050730.

ground state $J = 9/2$ for gas of $T = 2600 \text{ K}$, $n_i/n_{9/2}$ using the PopRatio software package (Silva & Viegas 2002). Figures 6 and 7 show the model predictions for excited Fe^+ and Si^+ respectively. Observations of these excited ions found in the GRB051111 progenitor environment are indicated in dotted curves.

Based on excited Fe^+ , we find that $n_e = 900\text{--}1500 \text{ cm}^{-3}$.

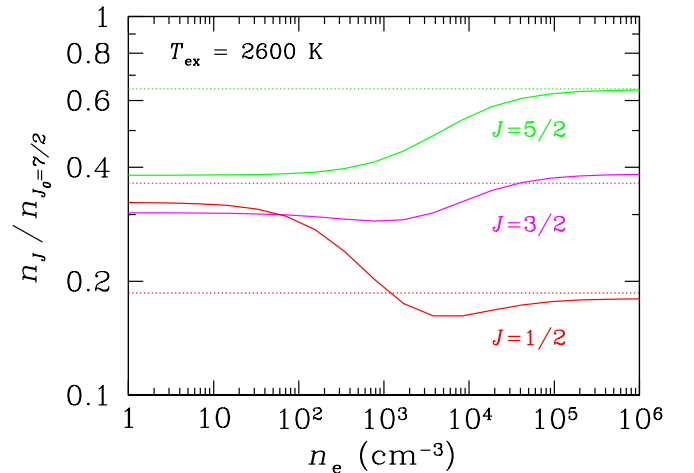


FIG. 6.— Abundance of the $J < 7/2$ Fe^+ excited states relative to the $J = 7/2$ state for $T = 2600 \text{ K}$ as a function of electron density. The solid curves describe the predictions of these ratios from the software package PopRatio (Silva & Viegas 2002). The dotted horizontal lines show the abundance ratios for GRB 051111 (1σ uncertainty $< 10\%$) indicating $n_e > 5 \times 10^4 \text{ cm}^{-3}$.

Based on excited Si^+ , the models predict $n_e \sim 60 \text{ cm}^{-3}$, i.e. the derived n_e are inconsistent with one another. In ad-

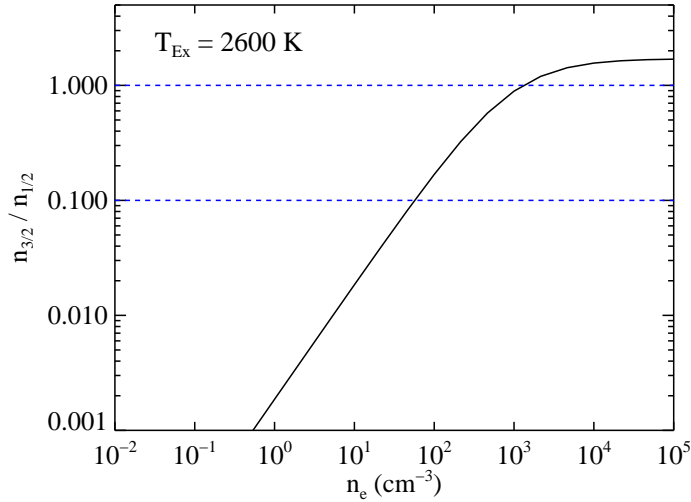


FIG. 7.— Predicted excitation of Si^+ (solid curve) as a function of electron density for a temperature $T = 2600$ K. The dashed line shows the observed ratio for GRB 051111 integrated over the entire line profiles shown in Figure 1. The observed value may be considered an upper limit and it suggests $n_e < 100 \text{ cm}^{-3}$.

dition, the same calculations predict that for excited Fe^+ states $n_{7/2}/n_{9/2} > 0.5$ under the assumption of local thermodynamic equilibrium (LTE) and no radiative pumping. This is inconsistent at $> 3\sigma$ with the observed column density ratio $N_{7/2}/N_{9/2}$, indicating $(n_{7/2}/n_{9/2})_{\text{obs}} = 0.05$ (Table 1). Because the Fe^+ states are Boltzmann distributed, this implies an n_e value greater than the critical electron density $n_e^C = A_{ji}/q_{ji}$ with q_{ji} the de-excitation rate. This implies a lower limit $n_e > 4 \times 10^5 \text{ cm}^{-3}$ which contradicts the density derived from the $n_i/n_{9/2}$ ratio. We have explored a wide range of n_e and T_{Ex} values and cannot resolve the discrepancy.

To reconcile the conflicting density constraints, we contend that a significant fraction ($\approx 90\%$) of the absorbing gas that gives rise to resonance transitions lies outside of the dense medium that gives rise to the fine structure transitions. This is supported by the discrepant absorption line profiles presented in Figure 3 for different Fe II transitions. We note that while the velocity profiles of the excited states track each other very closely, i.e. the relative abundance is constant over the $\pm 40 \text{ km s}^{-1}$ velocity interval, the profile for $J = 9/2$ transitions is significantly different from those of the fine-structure lines. This assessment is further supported by a Voigt profile fitting analysis of the Fe II transitions. We first model the line profiles of Fe II 2249 and 2260 with a single Voigt profile centered at $z = 1.54948$ using the VPFIT software package. We obtain a good solution with a Doppler parameter of $b = 10 \text{ km s}^{-1}$. Next, we fit this single component to the fine-structure transitions. Although the best-fit column densities agree with our AODM analysis, the single component solution is clearly a poor representation of the data (Figure 8). The fine-structure line-profiles require a two-component solution with component separation of $\delta v \approx 10 \text{ km s}^{-1}$.

In summation, the $J = 9/2$ line-profile is qualitatively different from the fine-structure lines indicating that ad-

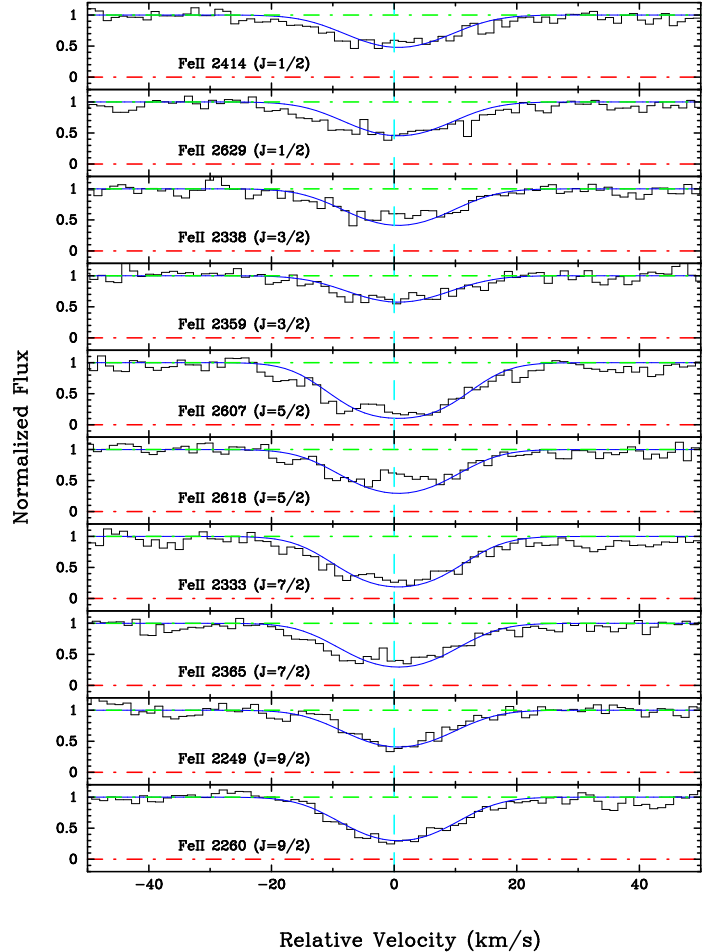


FIG. 8.— Velocity profiles of for a subset of the a^6D sextet of Fe^+ toward GRB 051111. The overplotted curve is a Voigt profile fit to the ground-state transitions ($J = 9/2$) and corresponds to $z = 1.54948$ and Doppler parameter $b = 10 \text{ km s}^{-1}$. While the model is a good description of these transitions, it is inconsistent with the observed line profiles of the excited states of Fe^+ . We argue, therefore, that only $\approx 10\%$ of the gas associated with the $J = 9/2$ state is co-spatial with the fine-structure states.

ditional contribution to the ground state from gas located along the sightline at a velocity near the centroid of the fine-structure lines. Indeed, one expects that the sightline to GRB 051111 penetrates a significant column density of ‘ambient’ ISM in the host galaxy given that GRB occur within the inner few kpc of the host (Bloom, Kulkarini & Djorgovski 2002). A scenario where $\approx 90\%$ of the ground-state Fe II and Si II gas is located in a different, lower-density region leads to a consistent electron density of $n_e \sim 10^5 \text{ cm}^{-3}$ for the excited ions.

We have repeated the analysis for fine structure transitions observed in GRB 050730 and find that the absorbing medium also has high density: $n_e > 10^3 \text{ cm}^{-3}$.

4. GASEOUS PROPERTIES AS CONSTRAINED BY NEUTRAL SPECIES

Additional constraints on the physical properties of the gas can be learned from the presence and absence of neutral species such as Fe^0 and Mg^0 . These species are unexpected even in a neutral hydrogen gas because their ionization potential is less than 1 Ryd. At the temperatures con-

sidered here $T < 10000$ K, the primary ionization mechanism for the atomic gas is photoionization; the collisional ionization rate is more than $10\times$ lower than the photoionization rate even at high gas density (Voronov 1997). The radiation field of interest here is confined to

$$8\text{ eV} < h\nu < 13.6\text{ eV}, \quad (4)$$

where the lower limit represents the ionization potential of these atoms, $h\nu > \text{IP}(\text{Mg}, \text{Fe}) \approx 8\text{ eV}$ and the upper limit is imposed by the optical thickness of the gas to photons with energy greater than 1 Ryd.

In principle, relative abundance measurements of Mg^0 , Fe^0 , Mg^+ , and Fe^+ (available for GRB 051111) can serve to constrain the density and temperature of the gas and/or reveal the intensity of the radiation field at $h\nu \approx 10\text{ eV}$. The analysis is complicated, however, by two issues. First, for those atomic species one detects (e.g. Mg^0), we do not know where this gas originates. For GRB 051111, we must consider two scenarios: (a) the neutral species originate primarily in the dense gaseous cloud that gives rise to the observed fine structure transitions and track $\approx 10\%$ of the gas that gives rise to the ground-state transitions (§ 3.3); and (b) the neutral species and resonance transitions share the same origin and track each other completely. Second, when examining scenario (a) one must consider the effects of the GRB event itself, i.e. the UV emission of the afterglow.

4.1. Fe^0

We first consider neutral Fe, which is rarely observed in the Galactic ISM (e.g. Welty, Hobbs & Morton 2003) and has never been observed in a damped $\text{Ly}\alpha$ system. Figure 1 shows that Fe I is not detected and we report an upper limit to the column density $N(\text{FeI}) < 10^{11.8}\text{ cm}^{-2}$. Under scenario (a), the key point to address is whether the absence of Fe^0 is consistent with the very large electron density implied by the fine-structure analysis. Neglecting the enhanced radiation from the GRB event itself and considering a gaseous cloud of $T = 2600$ K under photoionization equilibrium, we know that the abundance ratio between Fe^0 and Fe^+ follows

$$\frac{n_e}{n_\gamma} = 3 \times 10^5 \frac{n(\text{Fe}^0)}{n(\text{Fe}^+)}, \quad (5)$$

where n_γ is the total density of photons within the energy interval as defined in Equation 4. In the Galactic ISM, $n_{\gamma_0} \approx 0.005\text{ cm}^{-3}$ and the intensity of the radiation field is $G_0 = 1.6 \times 10^{-3}\text{ ergs cm}^{-2}\text{ s}^{-1}$ (Habing 1968). We therefore replace n_γ in Equation 5 by $0.005(G/G_0)\text{ cm}^{-3}$ where G characterizes the ambient radiation field of the GRB progenitor.

Following scenario (a), we derive $N(\text{Fe}^0)/N(\text{Fe}^+) < 10^{-2.4}$ over the $\pm 40\text{ km s}^{-1}$ interval at $z = 1.5495$. The relative abundance between Fe^0 and Fe^+ therefore yields an upper limit to n_e for a given radiation field,

$$n_e < 1200n_\gamma = 6.0 \frac{G}{G_0}. \quad (6)$$

Adopting the lower limit to n_e from the fine-structure analysis, we derive a lower limit on the intensity of the radiation field, $G/G_0 > 10^4$. The lack of Fe^0 therefore suggests that the gas is located near a bright UV source. We note that the presence of the GRB explosion itself is not

required to account for these observations, because large UV intensity is already expected near the GRB progenitor, i.e. a massive star emitting copious UV radiation. If we adopt an O star with $T_* = 40000$ K and $R = 10R_\odot$, then we estimate $n_\gamma \approx 10^{14}\text{ cm}^{-3}$ at the surface and therefore a sufficient UV flux for $r < 0.3\text{ pc}$ (ignoring dust).

4.2. Mg^0

Next, we examine limits to the radiation field based on the large Mg^0 column density. Mg^0 is commonly observed in quasar absorption line systems and in random sight-lines through the Milky Way (e.g. Churchill *et al.* 2000; Frisch *et al.* 1990). The main differences from Fe^0 are that Mg^0 has a smaller cross-section to 10 eV photons and that Mg^0 has a much higher recombination rate at $T > 5000\text{ K}$ where dielectronic recombination dominates (York & Kinahan 1979).

Similar to Equation 5, the detailed ionization balance at $T = 2600$ K follows

$$n_e = 200 \frac{n(\text{Mg}^0)}{n(\text{Mg}^+)} \frac{G}{G_0}, \quad (7)$$

where we have adopted the photoionization rate from Frisch *et al.* (1990) and the radiative and dielectronic recombination rates from Aldrovandi & Pequignot (1973) and Shull & van Steenberg (1982). Note that the total recombination rate varies by less than a factor of two from $T = 1000 - 6000$ K but is $\approx 10\times$ larger at $T = 10000$ K.

Constraints on the radiation field using Mg are weaker, because the Mg II doublet at 2800 \AA is heavily saturated and does not provide even a meaningful lower limit to $N(\text{Mg}^+)$. It is reasonable to assume, however, that $N(\text{Mg}^+) \approx N(\text{Si}^+)$ because (i) these elements have similar absolute abundances in many astrophysical environments; (ii) the singly ionized states should be dominant in this gas; and (iii) these elements deplete roughly the same amount onto dust grains. Here, we observe $N(\text{Mg}^0)/N(\text{Mg}^+) \sim N(\text{Mg}^0)/N(\text{Si}^+) \lesssim 10^{-1.2}$ and derive $N(\text{Mg}^0)/N(\text{Mg}^+) = 10^{-0.2}$ following scenario (a), leading to

$$n_e \approx 120 \frac{G}{G_0} \text{ cm}^{-3}, \quad (8)$$

where one can assume an order of magnitude uncertainty in the relation. Regardless, if we adopt the lower limit to n_e from the fine-structure analysis, we again derive a lower limit on the intensity of the radiation field, $G/G_0 > 10^3$. If we adopt the same model for Fe^0 gas near an O star, then we derive a lower limit to the distance of the absorbing medium at $r \approx 0.03\text{ pc}$ in order to reproduce the observed Mg^0 column density.

4.3. Proximity Effect of the Afterglow

The proximity of the neutral species to the GRB progenitor ($0.03\text{ pc} < r < 0.3\text{ pc}$ under the assumption of scenario (a), indicates that the afterglow of the burst must dominate the radiation field. Therefore, the location of the observed neutral species is likely to be further away from the GRB than the distance derived in the previous section. We can check this assertion by determining the radial extent of the GRB proximity effect for each ion of interest.

In particular, the afterglow of GRB 051111 reached an apparent magnitude $R = 13.3\text{ mag}$ at $t \approx 50\text{ s}$ following

the burst and exhibited significant flux in the observed ultraviolet (Poole *et al.* 2005). A preliminary analysis of the afterglow data indicate a decay constant $\alpha \approx -0.8$ and spectral index $\beta \approx -0.5$ (Butler *et al.* 2006, in prep.), i.e.,

$$F_\nu = 1.4 \times 10^{-25} \left(\frac{t}{50\text{s}} \right)^\alpha \left(\frac{\lambda}{6588\text{\AA}} \right)^{-\beta} \text{ erg cm}^{-2} \text{ s}^{-1} \text{ Hz}^{-1} \quad (9)$$

We calculate the number of photons over the period of $t = 50\text{s}$ to 3840s (when the Keck spectral observations commenced) that are capable of ionizing Mg^0 (ignoring the effects of differential dust extinction, which would suppress the true number of ionizing photons), and find that the GRB afterglow emitted $6.6 \times 10^{60} (\Omega/4\pi)$ photons of co-moving $h\nu = 7.7\text{eV}$ to 9.5eV . The cross-section of Mg^0 to ionization radiation at $h\nu = 9\text{eV}$ is $\sigma^\gamma(\text{Mg}^0) \approx 10^{-18} \text{ cm}^2$ (Verner *et al.* 1996). To completely ionize an optically thin slab of Mg^0 atoms requires a photon surface density of $1/\sigma^\gamma(\text{Mg}^0) = 10^{18} \text{ photons cm}^{-2}$. For GRB 051111, this condition is satisfied at $r < 100\text{ pc}$ from the event. Therefore, the detection of strong Mg I transitions demands that this gas originates in a region that is $r > 100\text{ pc}$ away from the GRB. Similar conclusions may be reached for any afterglow spectrum showing strong Mg^0 absorption.

Based on these arguments, we are compelled to adopt scenario (b), at least for the neutral Mg gas. In this case, the neutral species do not track excited ions but share the same origin as the resonance transitions. The underlying gas density is unknown under this scenario, but the detection of Mg^0 requires at least a modest electron density ($\gtrsim 1 \text{ cm}^{-3}$) and/or gas temperature $T > 5000\text{ K}$. Regarding the excited gas, however, the absence of significant Fe I absorption at these large densities implies the gas is found within 200 pc of the GRB event. Within this distance, radiation from the afterglow is sufficient to fully ionize any Fe^0 that may have been present.

In summary, the detection of a large column density of Mg^0 lends further support that a significant fraction of the neutral gas along the line of sight toward GRB 051111 is found at $r > 100\text{ pc}$ from the GRB and is therefore likely separate from the star-forming region of the progenitor. Furthermore, the observations clearly rule out a scenario with low density gas located within an active star forming region. We discuss the nature of this cloud and its implications in the following section.

5. DISCUSSION

Echelle spectroscopic observations of GRB afterglows have unveiled extreme physical conditions in the circumburst environment that are rarely seen even in the local ISM of the Milky Way. Our observations of two GRB sightlines show that the circumstellar medium is characterized by the following generic features. First, the large column density of H^0 and/or singly ionized heavy elements indicates that the gas is opaque to FUV photons, i.e. the gas is mostly neutral. Second, the large abundances of Si^+ and Fe^+ in the excited states indicate that the electron density exceeds $n_e = 10^3 \text{ cm}^{-3}$. Third, the population ratios between different excited states of Fe^+ indicates a gas temperature near $T \sim 2000 - 6000\text{ K}$.

The large gas density is only seen locally in either compact H II regions or giant molecular clouds, but the observed low ionization (see below) and the lack of H_2 to-

gether (Prochaska *et al.* 2006, in prep.) imply a unique GRB progenitor environment. Our analysis of both neutral species and excited ions has also identified two spatially distinct gaseous clouds that are responsible for producing the absorption spectrum of GRB 051111: one that gives rise to the observed fine-structure transitions and the other that gives rise to the majority of the observed resonance transitions. We have argued in § 4.2 that the excited ions are located within 200 pc of the GRB (whereas the majority gas is at distance $r > 100\text{ pc}$). Our study therefore represents the first observational analysis of the GRB environment on scales less than 10 pc .

Here we discuss further implications of the echelle observations for the GRB progenitor environment.

5.1. Physical Size of the Region Traced by Excited Fe^+

To estimate the total gas density n_{H} based on the estimated n_e requires knowledge of the ionization state of the absorbing gas traced by the excited Fe^+ . For GRB 050730, where we have a direct measurement of $N_{\text{HI}} = 10^{22.15} \text{ cm}^{-2}$ (Chen *et al.* 2005), the optical depth to ionizing radiation ($h\nu > 1\text{ Ryd}$) is $\tau \gg 1000$. While an O or B star (or the GRB itself) could significantly ionize a skin-layer on the outside of the cloud, the majority of the gas would remain neutral. Therefore, the hydrogen gas must be predominantly neutral and we can safely assume an ionization fraction $x < 10^{-2}$.

For GRB 051111, we estimate x based on the observed Al^{++} column density relative to the dominant ions. We find $\log[N(\text{Al}^{++})/N(\text{Fe}^+)] = -1.8$ dex. Assuming $N(\text{Al}^+)/N(\text{Fe}^+)$ is roughly equal to the solar ratio (Prochaska & Wolfe 2002), we infer $\log[N(\text{Al}^{++})/N(\text{Al}^+)] \approx -0.8$ dex. This is typical of damped Ly α systems with $N_{\text{HI}} \approx 10^{21} \text{ cm}^{-2}$ (Vladilo *et al.* 2001) and indicates the gas has a small ionization fraction. These arguments imply the gas associated with the fine-structure absorption is predominantly neutral and that the derived n_e values are lower limits to the hydrogen density. In summation, we infer $n_{\text{H}} > 10^7 \text{ cm}^{-3}$ for GRB 051111 and $n_{\text{H}} > 10^5 \text{ cm}^{-3}$ for GRB 050730.

Adopting these limits, we can estimate an upper limit to the size of the excited medium ℓ . For GRB 050730, the analysis implies $\ell = N_{\text{HI}}/n_{\text{H}} < 10^{17} \text{ cm}$, i.e., less than $1/30\text{ pc}$. For GRB 051111, the estimate is more difficult because we do not have a direct N_{HI} measurement. As Prochaska (2005) noted, the $N(\text{Zn}^+)$ value for this sightline implies an H I column density $N_{\text{HI}} > 10^{20.8} \text{ cm}^{-2}$. This is a conservative lower limit because the Zn II profiles are strongly saturated and because it assumes solar metallicity. We feel it is reasonable to adopt an upper limit of $N_{\text{HI}} = 10^{23} \text{ cm}^{-2}$ for the gas associated with the excited states (recall, this represents only $\approx 10\%$ of the ground-state Fe^+ ions). This implies $\ell < 10^{16} \text{ cm}$ or $1/300\text{ pc}$ for GRB 051111.

It is evident that the gas giving rise to the excited states has a much smaller size than the characteristic ‘clouds’ of the ISM (Hobbs 1974). The small dimension of this gas implies it must arise near the GRB event (at $r \sim \ell$) or have a nearly spherical covering fraction at large radii. Regarding the former point, we can estimate a lower limit to the radius from the explosion site at the time of the spectral observations. Based on our redshift measurements and the fluences reported from Swift (Markwardt *et al.*

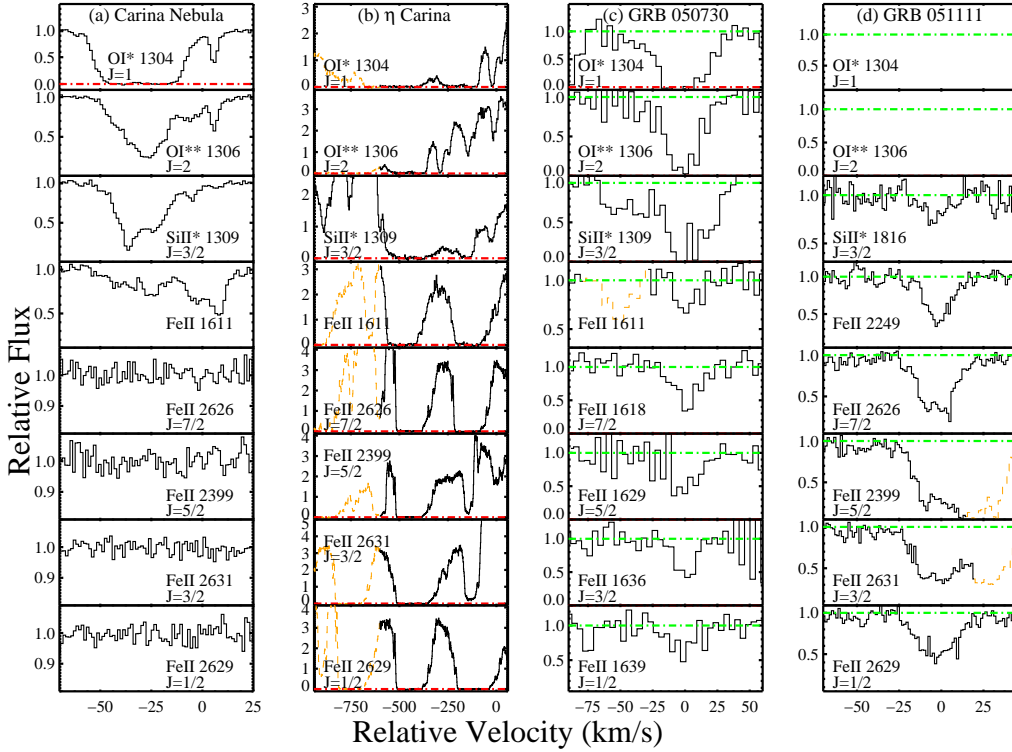


FIG. 9.— Velocity profiles of the gas originating in the nebula of η Carina (a) and along the direct sightline to η Carina (b) compared against GRB 050730 (c) and GRB 051111 (d). While both Carina sightlines exhibit very strong excited states of Si^+ and O^+ and also ground-state Fe II transitions, only the gas toward η Carina shows the excited Fe^+ states (Walborn *et al.* 2002; Gull *et al.* 2005; Nielsen, Gull & Vieira Kober 2005) also present toward the gamma-ray bursts.

2005; Krimm *et al.* 2005), the isotropic equivalent energies of the bursts are $E_{\text{iso}}[050730] = 3.9 \times 10^{53}$ erg and $E_{\text{iso}}[050730] = 6.9 \times 10^{52}$ erg; here we have assumed a bolometric k -correction = 3.0 (Bloom, Frail & Sari 2001). Under the traditional assumption of a homogeneous circumburst baryon density of $n = 3 \text{ cm}^{-3}$, the radii of the afterglow forward shock at the time of the spectral observations is:

$$R[051111] = 1.8 \times 10^{17} \left(\frac{n}{3 \text{ cm}^{-3}} \right)^{-1/4} \text{ cm} \quad (10)$$

$$R[050730] = 3.2 \times 10^{17} \left(\frac{n}{3 \text{ cm}^{-3}} \right)^{-1/4} \text{ cm} \quad (11)$$

If instead the density were equal to the lower limit on n_H the radii would be 1.3, 2.4×10^{16} cm for 051111 and 050730, respectively.

5.2. Thermal Balance

The most astonishing result of our analysis is that the gas has very high density yet relatively warm temperature. At these temperatures and density, several processes contribute to the cooling of the gas. These include Ly α cooling, cooling due to fine-structure states, and cooling from meta-stable states. For the physical conditions of the excited gas toward GRB 051111 ($T = 2600\text{K}$ and $n_e > 10^5 \text{ cm}^{-3}$), [Fe II] cooling dominates over Ly α cooling and other fine-structure gas. Using the coefficients given by Hollenbach & McKee (1989), we calculate a rate

of $n\Lambda_{[\text{FeII}]} = 4 \times 10^{-23} \text{ ergs s}^{-1} \text{ H}^{-1}$ assuming 1/10 solar metallicity and that 90% of the iron is locked into dust grains. This implies a cooling rate $t_{\text{cool}} \sim kT/(n\Lambda_{[\text{FeII}]}) < 500\text{yr}^{-1}$. Including the cooling by meta-stable states of O I would imply an even shorter cooling time. Therefore, the gas requires a substantial heat input in order for it to be in thermal equilibrium.

Heating in the vicinity of the GRB progenitor is presumably dominated by energetic electrons ejected from the photoionization of hydrogen and/or dust grains (e.g. Wolfire *et al.* 1995). The large heating rate required to balance efficient cooling due to high density therefore demands that the cloud be at close distance to the progenitor. In a future paper, we will attempt to construct a fully consistent thermodynamic model of the gas. For now, we stress that gas with $T \approx 3000\text{K}$ is generally not stable to perturbation. In the case considered here, the [Fe II] cooling curve is relatively insensitive to temperature variations but very sensitive to density changes. For example, an increase in n_H increases $n\Lambda_{[\text{FeII}]}$ and drives the gas to higher density and lower temperature until $T \ll 1000 \text{ K}$.

5.3. Kinematic Properties of the Circumburst Medium

The high resolution observations of GRB 051111 and GRB 050730 have also revealed detailed kinematic characteristics of the excited gas. The most notable, common characteristic is that the gas is confined to a small velocity width, with a FWHM of $\Delta v \approx 20 \text{ km s}^{-1}$ for each sightline. At temperature $T = 3000 \text{ K}$, the expected ther-

mal velocity width of Fe is $\sim 1.5 \text{ km s}^{-1}$, which is much smaller than the observed absorption line width. This indicates that the observed velocity width is dominated by the bulk motion of the gas. If we interpret the physical origin of the gas in terms of a shock interface (e.g. van Marle, Langer & Garcia-Segura 2005), then this velocity width characterizes a turbulent velocity field of $v_{\text{turb}} \sim 20 \text{ km s}^{-1}$.

As more burst afterglows are observed at high resolution, the diversity of the sightlines will almost certainly be an important clue for constraining the progenitors (Ramirez-Ruiz *et al.* 2005). Already, we note a significant contrast with GRB 021004, where high-velocity blueshifted line absorption features were taken as evidence of Wolf-Rayet outflow or radiative acceleration from the burst (Mirabal *et al.* 2003; Schaefer 2003). The absence of such features in our two spectra might lead credence to the notion that such features not a local effect, but were due to infall around the host galaxy of GRB 021004 (van Marle, Langer & Garcia-Segura 2005). Future time-resolution, high resolution spectroscopy may reveal evidence for velocity and column depth changes during the early stages of the afterglow, which would place more explicit constraints on the nature and location of the absorption material relative to the burst.

5.4. The Nature of the GRB Progenitor

Fe II fine-structure lines have never been observed in the ambient ISM of any known galaxies, because the ambient ISM has insufficient density at warm temperature to produce these excited states, and the typical cold cloud has too low electron density. This is consistent with identifications of strong Fe II fine structure transitions in extremely high density environments in the Milky Way, such as η Carinae (Gull *et al.* 2005; Nielsen, Gull & Vieira Kober 2005) and the circumstellar disk of β Pictoris (Lagrange-Henri, Vidal-Madjar & Ferlet 1988).

The resemblance between the circumburst environment of the two GRBs and η Carinae is particularly interesting, because of the possible Wolf-Rayet nature of the progenitor stars. Figures 9a,b show observations of excited ions along two sightlines of $1'$ apart toward η Carinae compared with the GRB profiles (c,d). Saturated Fe II fine-structure transitions span $\approx 500 \text{ km s}^{-1}$ along the sightline toward η Carinae and imply a gas density of $n \sim 10^7 \text{ cm}^{-3}$ (Gull *et al.* 2005). Meanwhile, Fe^+ ions are absent at $1'$ angular distance even though one identifies strong absorption from excited states of Si^+ and neutral oxygen. At 7500 light-years distance, the difference in the absorption line strengths between the two lines of sight indicates a very large density fluctuation on scales of less than $2/3 \text{ pc}$ in the η Carina nebula. This is consistent with the estimated size of the dense cloud that gives rise to the fine structure transitions.

By drawing analogy with the Milky Way, we find evidence again supporting the argument that the excited Fe^+ ions originate in the environment local to GRB 051111 and GRB 050730, e.g. the circumstellar material associated with the progenitor or the local ISM swept up by a massive stellar wind. We note that additional GRB spectroscopy will allow us to investigate the covering fraction of gas with the very high densities revealed for GRB 050730

and GRB 051111. We note that the fraction is not 100% (the gas toward GRB 050820 does not exhibit Fe II fine-structure absorption; Prochaska *et al.* 2006, in prep.) but current results indicate a very high incidence, suggestive of an isotropic wind from the GRB progenitor.

Approaching nine years since the start of the afterglow revolution of GRBs, studies probing the physical nature of the bursts, afterglows and progenitors proceed apace. Still, the promise of using GRBs as unique tools to probe the universe is only just becoming realized. The present study falls squarely in the interface between two broad endeavors. As a tool, we have shown how these two GRB afterglows provide unique extragalactic sightlines. Owing to the large redshift, the suite of Fe and Mg lines are easily accessible to optical spectrographs from the ground and have allowed us to probe the environments of extreme star formation in Wolf-Rayet stars, something not possible with ground-based spectroscopy of Galactic sightlines. In the context of GRB progenitors, these spectra, in concert with photometry of the afterglows, provide a detailed glimpse of the chemical enrichment history down radii approaching the afterglow radiation front.

The authors wish to recognize and acknowledge the very significant cultural role and reverence that the summit of Mauna Kea has always had within the indigenous Hawaiian community. We are most fortunate to have the opportunity to conduct observations from this mountain. We are grateful to Grant Hill, Derek Fox and Barbara Schaefer for their roles in obtaining the Keck/HIRES data of GRB 050111 and I. Thompson for obtaining the Magellan/MIKE data of GRB 050730. The authors would like to thank C. McKee, N. Walborn, T. Gull, K. Sembach, A. Wolfe, B. Mathews, D. York, D. Welty, C. Howk, and G. Blumenthal for helpful discussions. We give special thanks to N. Walborn and T. Gull for providing HST/STIS ultraviolet spectra of the carnia nebula and η carina. We thank Weidong Li and Nat Butler for providing preliminary results of the optical photometry of GRB 050111. J.X.P., J.S.B., and H.-W.C. are partially supported by NASA/Swift grant NNG05GF55G.

REFERENCES

- Aldrovandi, S. M. V. and Pequignot, D. 1973, *A&A*, 25, 137.
 Bahcall, J. N. and Wolf, R. A. 1968, *ApJ*, 152, 701.
 Berger, E. *et al.* 2005, ArXiv Astrophysics e-prints.
 Bernstein, R. *et al.* 2003, in *Instrument Design and Performance for Optical/Infrared Ground-based Telescopes*. Edited by Iye, Masanori; Moorwood, Alan F. M. Proceedings of the SPIE, Volume 4841, pp. 1694-1704 (2003), 1694.
 Bloom, J. S., Frail, D. A., and Sari, R. 2001, *AJ*, 121, 2879.
 Bloom, J. S., Kulkarni, S. R., and Djorgovski, S. G. 2002, *AJ*, 123, 1111.
 Bloom, J. S. *et al.* 2002, *ApJ (Letters)*, 572, L45.
 Chen, H.-W. *et al.* 2005, *ApJ*, 634, L25.
 Churchill, C. W. *et al.* 2000, *ApJS*, 130, 91.
 Frisch, P. C. *et al.* 1990, *ApJ*, 357, 514.
 Gull, T. R. *et al.* 2005, *ApJ*, 620, 442.
 Habing, H. J. 1968, *Bull. Astron. Inst. Netherlands*, 19, 421.
 Hall, P. B. *et al.* 2002, *ApJS*, 141, 267.
 Hill, G. *et al.* 2005, *GRB Circular Network*, 4255, 1.
 Hobbs, L. M. 1974, *ApJ*, 191, 395.
 Hollenbach, D. and McKee, C. F. 1989, *ApJ*, 342, 306.
 Howk, J. C., Wolfe, A. M., and Prochaska, J. X. 2005, *ApJ*, 622, L81.
 Jenkins, E. B. 1996, *ApJ*, 471, 292.

Krimm, H. *et al.* 2005, GRB Coordinates Network, 4260, 1.
 Lagrange-Henri, A. M., Vidal-Madjar, A., and Ferlet, R. 1988, A&A, 190, 275.
 Markwardt, C. B. *et al.* 2005, GRB Coordinates Network, 3715, 1.
 Mirabal, N. *et al.* 2003, ApJ, 595, 935.
 Nielsen, K. E., Gull, T. R., and Vieira Kober, G. 2005, ApJS, 157, 138.
 Paczyński 1998, in Gamma Ray Bursts: 4th Huntsville Symposium, volume 428, (Woodbury, New York: AIP), 783.
 Penprase, B. E. *et al.* 2005, ArXiv Astrophysics e-prints.
 Perna, R. and Loeb, A. 1998, ApJ, 501, 467.
 Poole, T. *et al.* 2005, GRB Circular Network, 4263, 1.
 Prochaska, J. 2005, GRB Circular Network, 4271, 1.
 Prochaska, J. X. and Wolfe, A. M. 2002, ApJ, 566, 68.
 Ramirez-Ruiz, E. *et al.* 2005, ApJ, 631, 435.
 Sarazin, C. L., Rybicki, G. B., and Flannery, B. P. 1979, ApJ, 230, 456.
 Savage, B. D. and Sembach, K. R. 1991, ApJ, 379, 245.
 Savaglio, S., Fall, S. M., and Fiore, F. 2003, ApJ, 585, 638.
 Schaefer, B. E. 2003, ApJ (*Letters*), 583, L67.
 Shull, J. M. and van Steenberg, M. 1982, ApJS, 48, 95.
 Silva, A. I. and Viegas, S. M. 2002, MNRAS, 329, 135.
 Stanek, K. Z. *et al.* 2003, ApJ (*Letters*), 591, L17.
 van Marle, A.-J., Langer, N., and Garcia-Segura, G. 2005a, ArXiv Astrophysics e-prints.
 van Marle, A.-J., Langer, N., and Garcia-Segura, G. 2005b, astro-ph/0507659.
 Verner, D. A. *et al.* 1996, ApJ, 465, 487.
 Vink, J. S. 2005, ArXiv Astrophysics e-prints.
 Vladilo, G. *et al.* 2001, ApJ, 557, 1007.
 Vogt, S. S. *et al.* 1994, in Proc. SPIE Instrumentation in Astronomy VIII, David L. Crawford; Eric R. Craine; Eds., Volume 2198, p. 362, 362.
 Voronov, G. S. 1997, Atomic Data and Nuclear Data Tables, 65, 1.
 Vreeswijk, P. M. *et al.* 2004, A&A, 419, 927.
 Walborn, N. R. *et al.* 2002, ApJS, 140, 407.
 Welty, D. E., Hobbs, L. M., and Morton, D. C. 2003, ApJS, 147, 61.
 Wijers, R. A. M. J. 2001, in Gamma-Ray Bursts in the Afterglow Era, Proceedings of the International workshop held in Rome, CNR headquarters, 17–20 October, 2000, ed. Enrico Costa, Filippo Frontera, and Jens Hjorth, (Berlin Heidelberg: Springer), 306.
 Wolfire, M. G. *et al.* 1995, ApJ, 443, 152.
 Woosley, S. E. 1993, ApJ, 405, 273.
 York, D. G. and Kinahan, B. F. 1979, ApJ, 228, 127.

TABLE 1
 IONIC COLUMN DENSITIES FOR GRB 051111

Ion	J ^a	E _{low} cm ⁻¹	λ (Å)	f	log N	log N _{adopt}
Mg I		0	1747.794	.00908	14.71 ± 0.03	14.705 ± 0.03
		0	1827.935	.02390	> 14.46	
		0	2026.477	.11200	> 14.21	
Al III		0	1862.790	.26800	13.40 ± 0.02	13.397 ± 0.02
Si II	1/2	0	1808.013	.00219	> 15.87	> 15.870
	1/2	0	2335.123	.00000	< 17.20	
	3/2	287	1816.928	.00166	14.82 ± 0.08	14.817 ± 0.08
Fe I		0.	2484.021	.55700	< 11.76	< 11.758
Fe II	9/2	0	2249.877	.00182	15.16 ± 0.02	15.198 ± 0.01
	9/2	0	2260.780	.00244	15.22 ± 0.01	
	7/2	385	2333.516	.06917	13.89 ± 0.01	13.900 ± 0.01
	7/2	385	2365.552	.04950	13.89 ± 0.01	
	7/2	385	2383.788	.00517	13.96 ± 0.10	
	7/2	385	2389.358	.08250	13.93 ± 0.02	
	7/2	385	2626.451	.04410	< 13.96	
	5/2	668	2328.111	.03555	13.69 ± 0.02	13.709 ± 0.01
	5/2	668	2607.866	.11800	13.71 ± 0.02	
5/2	668	2618.399	.05050	13.73 ± 0.02		
3/2	863	2338.725	.09250	13.44 ± 0.02	13.459 ± 0.01	
3/2	863	2359.828	.05727	13.51 ± 0.03		
3/2	863	2621.191	.00392	< 13.92		
1/2	977	2345.001	.15750	13.10 ± 0.03	13.174 ± 0.01	
1/2	977	2414.045	.17550	13.18 ± 0.02		
1/2	977	2622.452	.05600	13.13 ± 0.06		
1/2	977	2629.078	.17300	13.23 ± 0.02		

^aJ value for ions with excited states. E_{low} is the energy above the ground state.

^bAlthough the statistical uncertainty is as low as 0.01 dex in several cases, we adopt a minimum uncertainty of 5% in the analysis.

TABLE 2
 IONIC COLUMN DENSITIES FOR GRB 050730

Ion	J ^a	E _{low} cm ⁻¹	λ (Å)	f	log N	log N _{adopt}
Fe II	9/2	0	1608.451	.05800	> 14.72	14.984 ± 0.12
	9/2	0	1611.200	.00136	14.98 ± 0.12	
	7/2	384	1618.468	.02140	14.26 ± 0.06	14.288 ± 0.04
	7/2	385	1621.686	.03810	14.34 ± 0.07	
	5/2	668	1629.160	.03670	14.12 ± 0.07	14.123 ± 0.07
	3/2	863	1634.350	.02050	13.95 ± 0.11	13.922 ± 0.06
	3/2	863	1636.331	.04050	13.91 ± 0.07	
	1/2	977	1639.401	.05790	13.65 ± 0.07	13.647 ± 0.07

^aJ value for ions with excited states. E_{low} is the energy above the ground state.

^bAlthough the statistical uncertainty is as low as 0.01 dex in several cases, we adopt a minimum uncertainty of 5% in the analysis.